euronoise

Measurements of the bending moment at boundaries of a structure

Simon Chesne[a], Baptiste Chomette[b] and Charles Pezerat[c]

[a]LaMCoS - INSA-Lyon - CNRS UMR5259, 18-20, rue des Sciences, Bâtiment Jean d'Alembert, F-69621 Villeurbanne, France
[b]LaMCoS - INSA-lyon - CNRS UMR5259, 18-20, rue des Sciences, Bâtiment Jean d'Alembert, F-69621 Villeurbanne, France
[c]Laboratoire Vibrations Acoustique - INSA Lyon, 25 bis avenue Jean Capelle, Bâtiment Saint-Exupéry, F-69621 Villeurbanne cedex, France
simon.chesne@insa-lyon.fr

In the vibration transmission process, the part due to the moment excitation is often neglected, because of the difficulty to measure it, even if it is sometimes an important term. Indeed, several studies show that the influence of the moment in structure borne power transmission can be higher than simple force. Moment measurement or identification is an old problem especially at boundaries. It has been mainly investigated in mobility methods. In fact, bending moment expression can be seen as spatial derivatives of displacements. These derivatives can be approximated from measured displacements but two major difficulties appear: derivatives are highly sensitive to measurement errors and the usual methods used to obtain them (finite differences, modal approach, etc.) are not well adapted at boundary points. In this paper, two different moment identification methods are investigated where the considered structure is a beam. The first approach was already developed by authors; the second method is based on the use of particular shapes of piezoelectric patches. These methods are numerically implemented allowing us to compare and discuss on results.

1 Introduction

The identification of sources exciting structures from indirect measurement is of great practical interest, and several papers have addressed this problem. When forces inject or dissipate energy, structural intensity techniques (see for example [1, 2]) give a quantification of the power flow inside the structure due to flexural wave motions. Alternative techniques, like RIFF [3, 4], propose to compute the exciting force distribution using the motion equation of the structure. In all cases, the searched quantities depend on the spatial derivatives of the displacements. Moreover, obtaining these terms implies two major problems: they present a high sensitivity to the uncertainties of measurement and it is difficult to obtain them at structure boundaries. These boundaries being often the transmission ways of vibrations, measurement at these points is a major issue in source identification. Moreover, moment excitations or moment measurements present intrinsic practical difficulties, and are often disregarded. Various studies show its importance [5, 6] and other shows the difficulties to characterize such quantity [7]. Also, bending moments are quantities proportional to spatial derivatives of displacements and classical characterization methods using finite difference schemes are not suitable at boundaries.

In a prior article [8], boundary shear forces and bending moments of a beam were determined using a weak form of the motion equation. The principle consists in multiplying the equation of motion by a test function and integrating it through several integrations by part, so that the shear force and/or the bending moment can be extracted at one boundary of the integration domain by a spatial weighted average. Finally, the method remains to the integration of the displacement multiplied by an analytical function. Until now, this last integration is implemented by a discretization where displacements are measured with classical sensors like accelerometers, laser vibrometers...

Nevertheless, in such methods, the discretization introduces an approximation depending on the numerical method used to compute the integration. In this present work, a continuous approach is proposed using distributed sensors made by piezoelectric films or patches avoiding the discrete integral calculation. Indeed, the output of a piezoelectric sensor is a weighted average of the surface strains in the region covered by the electrodes on the patches. In the literature, spatially distributed piezoelectric are often used has sensor sensitive to a mode or a group of natural mode [9, 10], tailoring the patch (or electrode) shape.

In this paper, this new technique is proposed for bending moment measurement at boundaries of a beam submitted to flexural motion. Theory and numerical simulations of bending moment measurement using discrete [8] and continuous approaches are presented and compared. Both are based on the weak form of the equation of motion and use particular test functions. On one side, the test function constitutes weights in the discrete measured displacement. On the other side, the test function is used to design the piezoelectric patch shapes.

2 Basic equations of the system

In the following, the transverse vibrations of a beam is considered with the standard Euler-Bernoulli theory and the displacements $w(x,t)$ are described in an harmonic motion:

$$w(x,t) = w(x)e^{j\omega t} \tag{1}$$

where ω the angular frequency. For the sake of simplicity, the time dependence $e^{j\omega t}$ is omitted. The aim of this paper is to identify the boundary bending moment M from various measurements on a beam. When the beam is driven by an harmonic excitation, the analytic expression of M is [11]:

$$M(x) = EI\frac{\partial^2 w}{\partial x^2}(x) \tag{2}$$

where E is the complex Young modulus and I the flexural inertia of the beam.

Also, with Euler-Bernoulli assumptions, the dynamic motion equation can be written as:

$$EI\frac{\partial^4 w}{\partial x^4}(x) - \rho S\omega^2 w(x) = F(x) \tag{3}$$

where ρ is the mass density, S the section of the beam and $F(x)$ the exciting force distribution.

3 Basic equations of a piezoelectric sensor

In this section the same notations as in the IEEE standard on piezoelectricity is used. For a piezoelectric material, the

electrical and mechanical constitutive equations are coupled and can be written:

$$T = c^E S - dc^E E \tag{4}$$

$$D = dc^E S + \varepsilon^S E \tag{5}$$

where T is the stress vector, S is the strain vector, E the electric field vector and D the dielectric displacement vector. These physical quantities are linked by c^E the Young's modulus (elasticity matrix) under a constant electric field, ε^S the permittivity matrix under a constant strain, and d a piezoelectric constant matrix relating the strain to the electric field in the absence of mechanical stress.

Let us consider a laminar sensor with a short-circuited electrodes, so that a zero electric field is enforced ($E=0$). Equation (5) becomes:

$$D = dc^E S \tag{6}$$

In this study, only the transverse vibrations of the beam are taken into account. Consequently, the constant d is reduced to its d_{31} component representing an extension in the beam principal direction.

Figure 1 presents the piezoelectric patch characteristics used in this study where b and $2h$ are the beam width and thickness, $b_p(x)$ and h_p are the patch width and thickness. The electrode covers the whole patch surface.

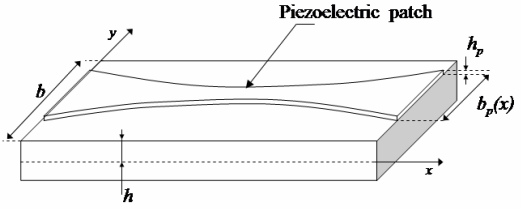

Fig. 1: Piezoelectric laminar sensor, stuck on a beam structure.

Assuming that a constant strain over the thickness of the patch (i.e. $h_p << h$), the Eq.(6) becomes:

$$D(x,t) = -d_{31} c^E h \frac{d^2 w}{dx^2}(x,t) \tag{7}$$

The corresponding electric charge is equal to the integral of the electric displacement over the patch area and can be written:

$$Q(t) = \int_0^a D(x,t) b_p(x) dx \tag{8}$$

If the polarization profile is uniform, d_{31} is constant and can be outside the integral:

$$Q(t) = -d_{31} c^E h \int_0^a \frac{d^2 w}{dx^2}(x,t) b_p(x) dx \tag{9}$$

When a charge amplifier is used (see figure 2), the output voltage is proportional to the electric charge in the electrode depending on the integral of the curvature weighted by $b_p(x)$.

$$v(t) = -\frac{Q(t)}{C_a} = \frac{d_{31} c^E h}{C_a} \int_0^a \frac{d^2 w}{dx^2}(x,t) b_p(x) dx \tag{10}$$

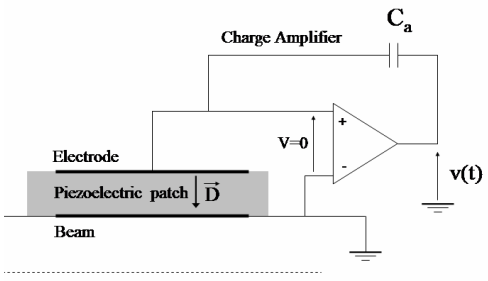

Fig. 2: Piezoelectric patches connected to charge amplifier

4 Bending moment identification

4.1 Using displacement measurements

In [8], authors have shown that using the weak form of Eq.(3) and a particular test function $\eta_M(x)$, it is possible to compute the bending moment at one boundary *(for example x=0)* using only displacement measurements. Without excitation in the integration domain *[0,a]* , the boundary bending moment at x=0 can be obtained by:

$$M(0) = \int_0^a w(x)[\rho S\omega^2 \eta_M(x) - EI \frac{\partial^4 \eta_M}{\partial x^4}(x)]dx \tag{11}$$

$$\text{with} \quad \eta_M(x) = x - 20\frac{x^4}{a^3} + 45\frac{x^5}{a^4} - 36\frac{x^6}{a^5} + 10\frac{x^7}{a^6} \tag{12}$$

In practice, the integral in Eq.(11) is discretized, so that $w(x)$ is measured in a finite number of points. This constitutes the only approximation error.

4.2 Using piezoelectric patches

Here, the approach uses also the weak form of the equation of motion, but the test function is substituted by a analytic function derived two times $\frac{\partial^2 \psi}{\partial x^2}(x)$:

$$\int_0^a \frac{\partial^2 \psi}{\partial x^2}(x)[EI \frac{\partial^4 w}{\partial x^4}(x) - \rho S\omega^2 w(x)]dx = 0 \tag{13}$$

Eq.(13) can be transformed using integrations by parts, leading to the following result:

$$\begin{aligned} &EI \frac{\partial^3 w}{\partial x^3}(a)\frac{\partial^2 \psi}{\partial x^2}(a) - EI \frac{\partial^3 w}{\partial x^3}(0)\frac{\partial^2 \psi}{\partial x^2}(0) - M(a)\frac{\partial^3 \psi}{\partial x^3}(a) \\ &+M(0)\frac{\partial^3 \psi}{\partial x^3}(0) - \rho S\omega^2 w(a)\frac{\partial \psi}{\partial x}(a) + \rho S\omega^2 w(0)\frac{\partial \psi}{\partial x}(0) \\ &+\rho S\omega^2 \frac{\partial w}{\partial x}(a)\psi(a) - \rho S\omega^2 \frac{\partial w}{\partial x}(0)\psi(0) \\ &= \int_0^a \frac{\partial^2 w}{\partial x^2}(x)[\rho S\omega^2 \psi(x) - EI \frac{\partial^4 \psi}{\partial x^4}(x)]dx \end{aligned} \tag{14}$$

In Eq.(14) boundary bending moments $M(0)$ appears in the fourth term. Then, M(0) can be isolated when a judicious choice of a the particular function $\psi(x)$ is made to force other terms to zero. This can be done if $\psi(x)$ satisfies the following conditions:

$$\begin{cases} \psi(0)=0 & \psi(a)=0 \\ \frac{\partial\psi}{\partial x}(0)=0 & \frac{\partial\psi}{\partial x}(a)=0 \\ \frac{\partial^2\psi}{\partial^2 x}(0)=0 & \frac{\partial^2\psi}{\partial^2 x}(a)=0 \\ \frac{\partial^3\psi}{\partial^3 x}(0)=1 & \frac{\partial^3\psi}{\partial^3 x}(a)=0 \end{cases} \quad (15)$$

Indeed, when these conditions are satisfied, Eq.(14) becomes:

$$M(0)=\int_0^a \frac{\partial^2 w}{\partial x^2}(x)[\rho S\omega^2\psi(x)-EI\frac{\partial^4\psi}{\partial x^4}(x)]dx \quad (16)$$

To satisfy conditions (15) a polynomial function is chosen. The lowest order solution is:

$$\psi(x)=\frac{1}{6}x^3-\frac{2}{3}\frac{x^4}{a}+\frac{x^5}{a^2}-\frac{2}{3}\frac{x^6}{a^3}+\frac{1}{6}\frac{x^7}{a^4} \quad (17)$$

$$\frac{\partial^4\psi}{\partial x^4}(x)=-\frac{16}{a}+120\frac{x}{a^2}-240\frac{x^2}{a^3}+140\frac{x^3}{a^4} \quad (18)$$

With these polynomial functions (represented in figure 3 and 4), expression (16) shows that the boundary bending moment at (x=0) can be computed with a spatial integration of the curvature $\frac{\partial^2 w}{\partial x^2}(x)$ weighted by an analytically known function ($\Psi(x)=\rho S\omega^2\psi(x)-EI\frac{\partial^4\psi}{\partial x^4}(x)$).

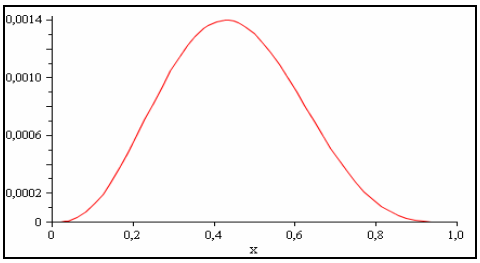

Fig. 3 : Test function $\psi(x)$

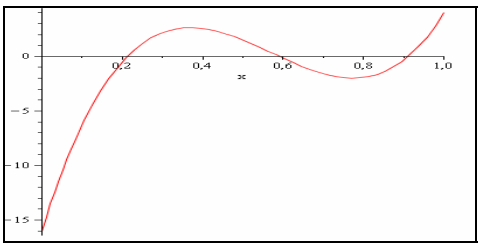

Fig. 4: Fourth derivative of $\psi(x)$

Now, by a comparison of equations (10) and (16), one can note that if the width $b_p(x)$ of the piezoelectric patch verifies the follow expression:

$$b_p(x)=\Psi(x)=\rho S\omega^2\psi(x)-EI\frac{\partial^4\psi}{\partial x^4}(x) \quad (19)$$

the output voltage becomes proportional to the bending moment at x=0:

$$v(t)=KM(0) \quad (20)$$

where K is a constant defined as $K=\frac{d_{31}c^E h}{C_a}$

Nevertheless, for practical reason, and in order to be frequency independent, two different patches will be used. The shapes of the piezoelectric patches are defined by the test functions $\psi(x)$ (patch A) and its fourth spatial derivative (patch B) (figure 3 and 4). Note that for the patch B, the sign of the width $b_p(x)$ is negative at given coordinates along the patch. This can be done by inversing the polarity of the strip. As an alternative, the part of the sensor with negative polarity can also be stuck on the opposite side of the beam.

Now, from Eq.(10), the bending moment $M(0)$ is quantified using two integrals corresponding to each patch:

$$M(0)=\rho S\omega^2\underbrace{\int_0^a \frac{\partial^2 w}{\partial x^2}(x)\psi(x)dx}_{\text{Patch A}}-EI\underbrace{\int_0^a \frac{\partial^2 w}{\partial x^2}(x)\frac{\partial^4\psi}{\partial x^4}(x)dx}_{\text{Patch B}} \quad (21)$$

The patch A is associated with the kinetic energy and is called “Mass Patch”. The patch B is associated with strain energy and is called “stiffness Patch”.

5 Numerical simulations

5.1 Step 1: Numerical setup - obtaining displacements and curvatuves of a beam

In this section, a clamped-free beam of length L excited by a harmonic force located at the point $X_f=0.8L$ is studied. To identify the bending moment at boundary point (x=0) with both approaches, the displacements and the curvatures are analytically computed.

The displacements are computed from a wave decomposition at each side of the excitation point:

$$\begin{aligned} w_1(x)&=A_1\cos(kx)+B_1\sin(kx)+C_1e^{-ikx}+D_1e^{ikx} \quad \text{for } x\in[0,X_f] \\ w_2(x)&=A_2\cos(kx)+B_2\sin(kx)+C_2e^{-ikx}+D_2e^{ikx} \quad \text{for } x\in[X_f,L] \end{aligned} \quad (22)$$

Where $w_1(x)$ (resp. $w_2(x)$) is the solution at the left hand side (resp. right hand side) of the excitation point, A_1, B_1, C_1, D_1, A_2, B_2, C_2, and D_2 are the wave amplitudes and k is the natural wavenumber, satisfying the dispersion equation:

$$k^4=\frac{\rho S}{EI}\omega^2 \quad (23)$$

The wave amplitudes are then computed in order to satisfy the 4 boundary conditions at $x=0$ and $x=L$ and the 4 continuity conditions at the excitation point $x=X_f$. Finally, the curvatures can be easily computed analytically as second spatial derivatives of displacements at each side of the excitation point.

5.2 Step 2: bending moment identification using displacement on a meshgrid

Because the displacements cannot be measured continuously along the beam, integral (11) is discretized. Here, the well known trapezoid integration method is chosen.

As expected using experimental data; the measured displacements are not exact. The goal of this simulation is

to see the influence of small perturbations on the identification. The bending moment reconstruction is made here from noisy displacements w^{noisy} obtained by:

$$w^{noisy}(x_i) = w^{exact}(x_i).\Delta w_m.e^{j\Delta\varphi} \tag{24}$$

where Δw_m is a Gaussian random real number with a mean value equal to unity and standard deviation equal to 1% of displacement magnitude. $\Delta\varphi$ is an another Gaussian random real number with a zero mean value, and a standard deviation 1 deg.

The bending moment reconstruction error level ε_M is now given by Eq. 25:

$$\varepsilon_M = 10\ln\left|\frac{M(0)}{EI\dfrac{\partial^2 w}{\partial x^2}(0)}\right| \tag{25}$$

where *M(0)* is the reconstructed bending moment. Then, the plot of ε_M obtained from exact displacements allows to see only the discretization errors whereas that obtained from noisy displacements shows all errors: discretization and effects of noise in data.

As shown in [8], the key parameter is the number of wavelengths contained in the integration domain. Indeed, the result remains unchanged whatever the driving frequency. Figure 5 presents the plots of ε_M using exact and disturbed displacements. In these calculations 20 integration points were used.

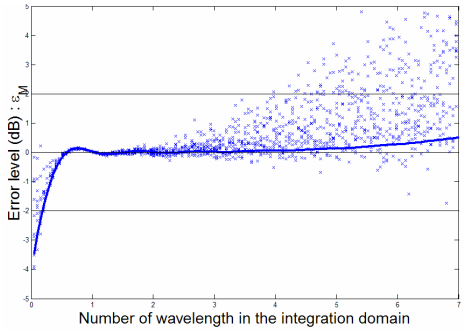

Fig. 5 : Error level between the simulation and the analytic bending moment using 20 points using exact displacements: solid line, using noisy displacements: crosses.

This method presents a huge error when the integration domain has less than one wavelength, due to the very high values of the test function fourth derivative when integration domain is very small. This error is drastically reduced when one wavelength is considered and increases softly when a higher number of wavelengths is included in the integration domain. It is due to the fact that when the number of wavelength included in the integration domain increase, the number of points per wavelength is reduced. Also, it is important to note that noise in data becomes non negligible in this last region, i.e. when the integration length is upper than 3 wavelengths.

5.3 Step 3: bending moment identification using designed piezoelectric patches

Here, the principle consists in using Eq.(21) where integrals have not to be discretized, because curvatures are directly integrated and weighted by the patches with their designed shapes. Consequently, integrals are numerically computed with a huge number of integration points in order to avoid errors due to the discretization. Figure 6 presents results obtained from exact curvatures. In figure 6.a, the error is always zero, because no assumptions are made at this step of the simulation. In figure 6.b, one can see the contributions of each patch computed from:

$$\varepsilon_{PatchA} = \frac{\rho S\omega^2\int_0^a \frac{\partial^2 w}{\partial x^2}(x)\psi(x)dx}{M_{analytic}(0)}$$
$$\varepsilon_{PatchB} = -\frac{EI\int_0^a \frac{\partial^2 w}{\partial x^2}(x)\frac{\partial^4 \psi}{\partial x^4}(x)dx}{M_{analytic}(0)} \tag{26}$$

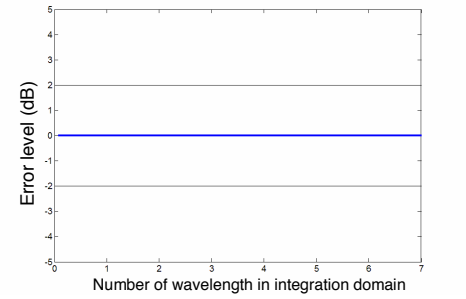

Fig. 6a: Error level between the simulation and the analytic bending moment.

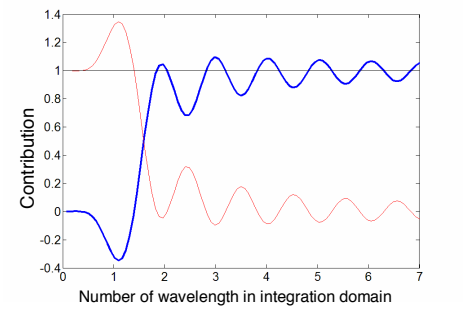

Fig. 6b: Contributions of each patch in bending moment identification (Patch A: thick line Patch B: thin line)

These contributions show how the information is distributed with respect to the wavelength in integration domain. When patch lengths are small (less than 1 wavelength), all the useful signal is delivered by the stiffness patch. Indeed, the stiffness patch is associated with the strain energy, which is the most important energy in the low frequency domain (where the natural wavelength is high). On the contrary, when patch lengths are bigger, the mass patch contribution becomes important, but the transfer is slow, with oscillations. In practice, small uncertainties can be introduced in the measurement technique principally due to the shape errors during the patch and electrode manufacturing or by bad bonding on the beam. To take into account these errors, arbitrary functions are introduced in Eq. (21):

$$M(0) = \rho S\omega^2 \underbrace{\int_0^a \frac{\partial^2 w}{\partial x^2}(x)\psi(x)\phi_1(x)dx}_{Patch\ A}$$
$$\underbrace{-EI\int_0^a \frac{\partial^2 w}{\partial x^2}(x)\frac{\partial^4 \psi}{\partial x^4}(x)\phi_2(x)dx}_{Patch\ B} \tag{27}$$

Functions $\Phi_1(x)$ and $\Phi_2(x)$ are spline interpolation functions using 20 points in the integration domain. Values are obtained from a Gaussian random real number with a mean value equal to zero and standard deviation equal to 1/100. Figure 7 illustrates one of these error functions.

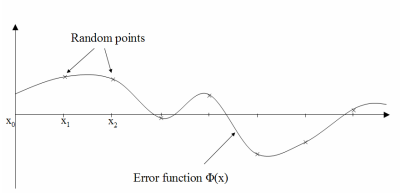

Fig. 7: Example of a part of an error function

Figures 8.a and 8.b present the error levels ε_M (defined in Eq.25) using disturbed integration and the contributions of each patch ε_{Patch_A} , ε_{Patch_B}. (defined in Eq.26).

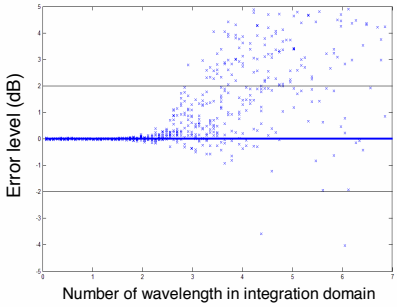

Fig. 8a: Error level between the simulation and the analytic bending moment using exact data: solid line, using noisy data: crosses.

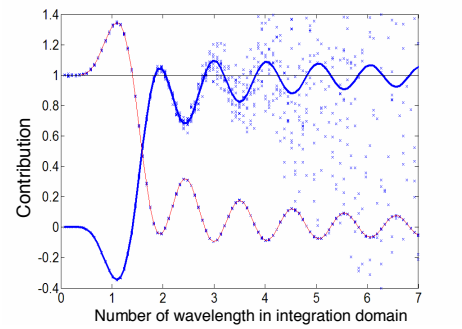

Fig. 8b: Contributions of each patch in bending moment identification (Patch A: thick line, Patch B: thin line)

When the integration domain is less than 3 wavelengths (Fig 8.a), the measurement method is very accurate uncertainties does not produce too important errors. Moreover, contrary to the previous approach a small integration domain gives very good identifications (see Fig 5 for comparison). Nevertheless, after this limit, huge errors appear. In Fig 8.b it is clear that the errors due to noise in data are particularly provided by the "mass patch". This phenomenon comes from the fact that the Mass Patch signal is a second temporal derivative. This is the reason why the errors are bigger when the integration length is large, i.e. when the wavelength is small in comparison with patch length. As an example, for a patch of length 10cm stuck on a steel beam with a section: 20*3mm^2, the frequency corresponding to a wavelength equal to 1/3 patch length is around 25000Hz. Finally, for this kind of structure and for low audible frequencies, a stiffness patch appears sufficient and the signal delivered should not be sensitive to internal defaults of the sensor.

6 Conclusion

Two boundary bending moment identification methods have been investigated by means of computer simulations in case of a clamped free beam. Both approaches are based on the weak form of the motion equation using particular test functions. The difference between both identifications is in there implementation. The first uses discrete measured displacements; so that approximations appear in the integral calculation particularly when the integration domain is very small or very large with respect to the wavelength. In the second implementation, the use of 2 piezoelectric patches with specific shapes issued from a test function allows to identify bending moments without discretization. Comparisons between numerical and noisy simulations between both approaches show that the use of patches presents a better regularizing aspect especially when the patch lengths are small.

References

[1] G. Pavic, "Measurement of structural borne wave intensity, part1: Formulation of the methods" , *J. Sound and Vibr.*49, 221-230, (1976)

[2] Noiseux, D. U., "Measurement of Power Flow in Uniform Beams and Plates," *J. Acoust. Soc. Am.*, 47, pp. 238–247 (1970).

[3] Pezerat, C., and Guyader, J.-L., "Two Inverse Methods for Localisation of External Source Exciting a Beam," *Acta Acoust*, 1(3), pp. 1–10. (1995)

[4] Pézerat C. and Guyader J-L "Force Analysis Technique: Reconstruction of Force Distribution on Plates" *Acta Acoustica*, 86, 322-332, (2000).

[5] G. Pavic, Q. Leclère 2007 "Moment excitation: an old problem revisited" Proceeding in INTER-NOISE 2007 Istanbul, Turkey 28-31 August. (2007).

[6] Fulford R. A., Petersson, B. A. T., "The role of moments on the vibration transmission in built-up structure", *J. Sound and Vibr.*227 (3), 479-510 (1999).

[7] Elliott, A., Moorhouse, A., Pavic, G., "Characterisation of a structure-borne sound source using independent and in-situ measurement" proceeding in ICA Madrid Spain, 2-7 sept. (2007)

[8] Chesné S., Pézerat C. and Guyader J-L "Identification of boundary forces in beams from measured displacements" *ASME J. Vibr. And Acoustic*, 128(6), 757-771, (2006).

[9] Tzou H. S., and Hollkamp J. J.;, "Collocated independent modal control with self-sensing orthogonal piezoelectric actuator (theory and experiment)" *Smart Mater. Struct.*, 3, 277-284 (1994).

[10] Preumont A., François A., De Man P., Piefort V., "Spatial filters in structural control", *J. Sound and Vibr.*265, 61-79. (2003)

[11] Guyader J-L "Vibration in continuous media", ISTE, 448p, (2006).